Available online at www.sciencedirect.com
ScienceDirect
Catalysis Today 118 (2006) 128–135
CATALYSIS TODAY
www.elsevier.com/locate/cattod

Evaluation of perovskites in hollow fibre and disk geometry in catalytic membrane reactors and in oxygen separators

J. Caro [a,*], H.H. Wang [a], C. Tablet [a], A. Kleinert [a], A. Feldhoff [a], T. Schiestel [b], M. Kilgus [b], P. Kölsch [c], S. Werth [d]

[a] *University of Hanover, Institute of Physical Chemistry and Electrochemistry, Callinstr. 3, D-30167 Hanover, Germany*
[b] *Fraunhofer Institute for Interfacial Engineering and Biotechnology (IGB), Nobelstr. 12, D-70569 Stuttgart, Germany*
[c] *Institute for Applied Chemistry Berlin-Adlershof (ACA), Richard-Willstätter-Str. 12, D-12489 Berlin, Germany*
[d] *Uhde GmbH, Friedrich-Uhde-Str. 15, D-44141 Dortmund, Germany*

Available online 10 July 2006

Abstract

Perovskite hollow fibre membranes of the composition $BaCo_xFe_yZr_{1-x-y}O_{3-\delta}$ (BCFZ) were prepared by a spinning process and subsequent sintering. The fibres were successfully tested in the production of pure oxygen and oxygen-enriched air as well as in a catalytic membrane reactor for the partial oxidation of methane to synthesis gas. In addition to BCFZ, for comparison perovskites of the composition $Ba_{0.5}Sr_{0.5}Co_{0.8}Fe_{0.2}O_{3-\delta}$ (BSCF) and $Ba_{0.5}Sr_{0.5}Zn_{0.2}Fe_{0.8}O_{3-\delta}$ (BSZF) as well as $SrCo_{0.8}Fe_{0.2}O_{3-\delta}$ (SCF) were prepared and tested. The atomic structure of the grain boundaries and their influence on oxygen transport are discussed. The thermal expansion coefficient is derived from *in situ* high temperature XRD.

Keywords: Hollow fibre; Disk geometry; Oxygen separator

1. Introduction

Twenty years after the pioneering papers of Teraoka et al. [1,2] who first reported the oxygen permeation through a perovskite membrane based on $La_{1-x}A_xCo_{1-y}Fe_yO_{3-\delta}$ there exists still no industrial application of perovskite type membranes. This lack of applicability is mainly due to (i) the long-time stability problems of perovskites, especially at low oxygen partial pressure and (ii) difficulties in the construction of high-temperature modules with gas-tight seals working near 850 °C.

Membrane development represents a frontier research area in chemical engineering, materials science and materials chemistry. The breakthrough in the wide application of organic polymer membranes in dialysis, natural gas treatment and treatment of refinery gas streams became possible through the availability of hollow fibre membranes. Consequently, increasing activities can be observed in the preparation of oxygen ion conducting membranes in a hollow fibre geometry. Examples are the pioneering papers from the groups of Li and co-workers [3–7] and Galavas and co-workers [8,9] as well as the papers by Schiestel et al. [10], Trunec [11], Luyten et al. [12], and Tablet et al. [13] showing that thin walled ceramic tubes can be prepared by spinning. The development of perovskite hollow fibre membranes is expected to trigger a similar development as was observed in the field of hollow fibre organic polymer membranes.

The aim of this paper is to study and to characterize the perovskite materials $BaCo_xFe_yZr_{1-x-y}O_{3-\delta}$ (BCFZ) to prepare user-friendly hollow fibres by spinning, and to give examples for the application of hollow fibres in membrane reactors and oxygen separators. Among the variety of perovskite compositions, the basic material BCFZ developed at the Dalian Institute of Chemical Physics of the Chinese Academy of Sciences was modified and chosen for fibre production because it represents a good compromise between a high oxygen flux and a good stability [14,15]. Other perovskite materials were prepared for comparison.

2. Experimental

The calcined BCFZ powder was spun into fibres as described in Section 3.1 and Ref. [10]. For comparison

* Corresponding author.
E-mail address: caro@pci.uni-hannover.de (J. Caro).

0920-5861/$ – see front matter
doi:10.1016/j.cattod.2005.12.015

$Ba_{0.5}Sr_{0.5}Co_{0.8}Fe_{0.2}O_{3-\delta}$ (BSCF) [16], $Ba_{0.5}Sr_{0.5}Zn_{0.2}Fe_{0.8}O_{3-\delta}$ (BSZF) [17,18], and $SrCo_{0.8}Fe_{0.2}O_{3-\delta}$ (SCF) [19] were prepared as well. The powders were uniaxially pressed into disks under 16 MPa for 5–10 min and subsequently sintered.

The crystal structures were characterized by *in situ* high-temperature X-ray diffraction (PHILIPS-PW1710) using Cu Kα radiation. The sample was tested in a high temperature cell (Bühler HDK 2.4 with REP 2000) with a heated Pt sample holder up to 1000 °C.

The microstructure of the perovskite membranes was investigated at different length scales. Secondary electron micrographs were taken using a field-emission scanning electron microscope (FE-SEM) of the type JEOL JSM-6700F at low voltages. High-resolution transmission electron microscopy (HRTEM), bright-field (BF) and dark-field (DF) imaging as well as selected area electron diffraction (SAED) was performed at 200 kV in a JEOL JEM-2100F-UHR that yields a point resolution better than 0.19 nm. An Oxford Instruments INCA-200-TEM system with an ultra-thin window was attached to the microscope that allowed elemental analysis by energy-dispersive X-ray spectroscopy (EDXS).

In the catalytic experiments and in the oxygen separation, two sealing techniques for the BCFZ fibres were applied: cold sealing of the fibres by silicon rubber rings outside the oven and hot sealing by a gold paste in the hot zone of the oven as shown in Fig. 1. A ceramic glass powder was used to seal the disk shaped membranes. For gas analysis, an *on line*-coupled HP Agilent 6890N equipped with a Carboxen 1000 column (Supelco) was used.

For the determination of the effective membrane area S (Eq. (1)) was used

$$S = \frac{\pi L(d_o - d_i)}{\ln(d_o/d_i)} \quad (1)$$

with d_o and d_i denoting the outer and inner diameters of the hollow fibre of the effective length L, respectively. When short cm-long pieces of the hollow fibre were sealed with the gold paste, the whole fibre was in the isothermal zone of the oven and the effective length L for permeation is identical with the real length of the fibre. However, when 30 cm long hollow fibres in a 24 cm long oven were studied, only 16 cm were assumed as the effective fibre length L since from measuring the temperature profile of the oven it is known that only the inner 16 cm of the oven have a temperature >500 °C.

3. Results and discussion

3.1. Membrane manufacture

BCFZ hollow fibre membranes were manufactured at the Fraunhofer Institute for Interfacial Engineering and Biotechnology (IGB) by phase inversion spinning (see Ref. [10]). A homogeneous slurry of a polymer solution and the BCFZ powder was obtained by ball milling up to 24 h with a solid content of 50–60 mass%. The slurry was spun through a spinneret and the obtained infinite green fibre was cut into 0.5 m long pieces before sintering the hollow fibres in a hanging position. By calcination above 1200 °C the length of 50 cm and the inner diameter of 1mm of the green fibres shrink to a length of about 30 cm and an inner diameter of about 0.50 mm. Fig. 2 shows the cross-sections of the green and sintered BCFZ hollow fibre membrane. The cross-section of the green hollow fibre shows an asymmetric columnar structure (Fig. 2a) which results from the diffusion and phase separation phenomena during the spinning process. This structure is still remained after sintering for 5 h above 1200 °C (Fig. 2b and c). Note the shrinking during the sintering process (see shrinking from Fig. 2a and b). The magnification of the outer surface of the hollow fibre (Fig. 2d) proved that the BCFZ membrane consists of grains of different size in the μm-region with clear grain boundaries. Tests with N_2 at room temperature showed that the hollow fibres were gas tight.

3.2. Grain boundaries and oxygen transport

The role of the grain boundaries on the oxygen transport through perovskite membranes, that is to say on their electronic and ionic conductivity, is only poorly understood and rarely studied [20,21]. Therefore, in this work pressed disks of BSCF with different concentrations of grain boundaries were prepared as model system to study the influence of grain boundaries on the oxygen transport.

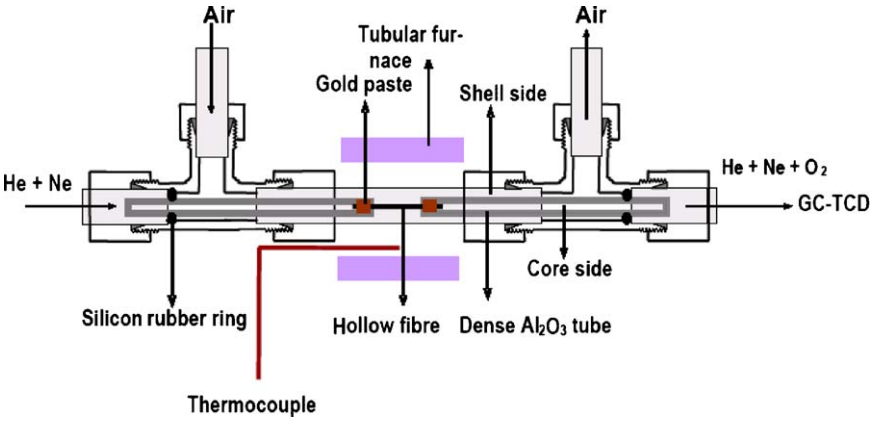

Fig. 1. Scheme of the one-hollow fibre catalytic membrane reactor and oxygen separator using gold paste for the hot sealing of the fibre.

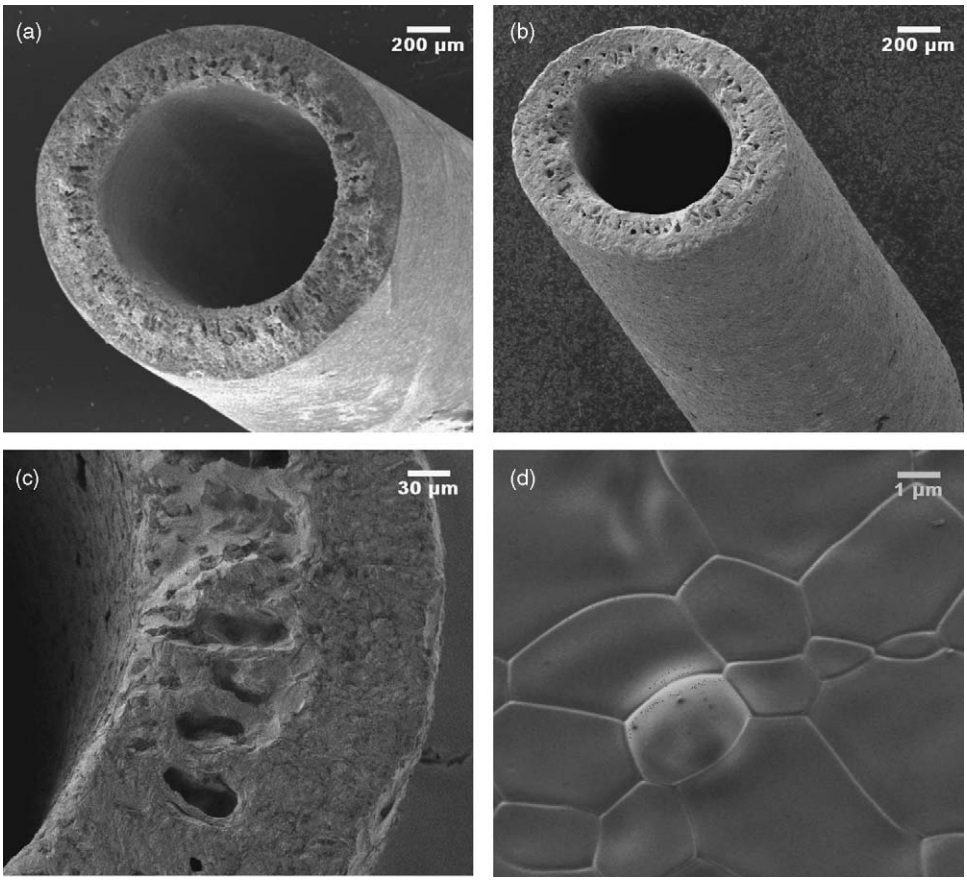

Fig. 2. SEM of the cross-sections of the green (a) and the sintered (b) BCFZ hollow fibres. Magnification of the cross-section of the sintered hollow fibre (c) and of its outer surface (d).

By increasing the sintering temperature and/or elongation of the sintering time (see Fig. 3), the crystallite size increases (Ostwald ripening) and the concentration of grain boundaries influencing mass transport is reduced. The grain size distribution has been determined from secondary electron micrographs by putting a threshold on an 8-bit gray scale that is implemented in the Image J software. Fig. 3 shows, that the oxygen flux through a BSCF pressed disk membranes which consist of small grains is retarded compared with the same sample containing larger grains (the enlarging of the grain size was achieved by higher sintering temperature and/or longer sintering time). The grain boundaries seem to represent

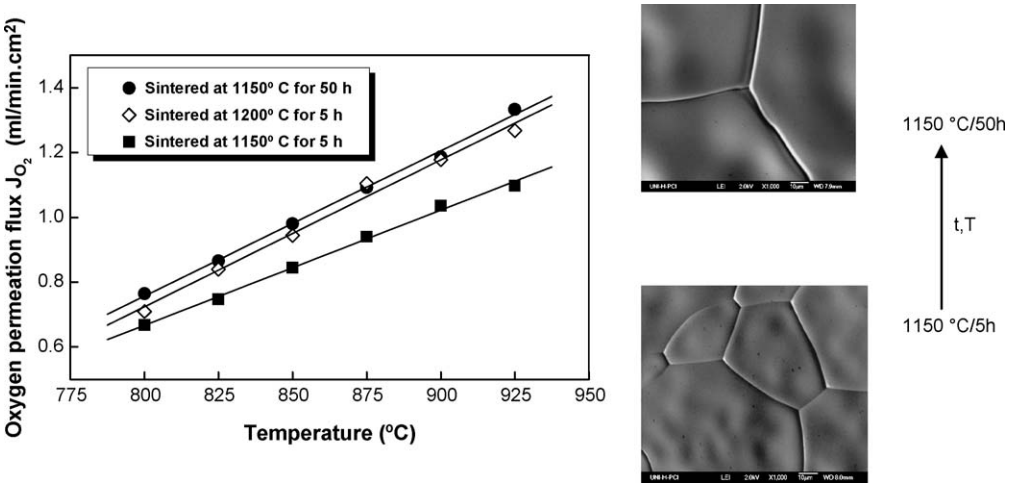

Fig. 3. Oxygen permeation through pressed BSCF discs of different grain size obtained by modifying the sintering conditions: 1150 °C/5 h, 40–60 μm; 1150 °C/50 h, 70–90 μm; 1200 °C/5 h, 70–90 μm. Experimental conditions: air flow = 150 ml/min; He as sweep = 30 ml/min; thickness of the discs = 1.0 mm; the oxygen partial pressures on the air side and on the sweep side are 0.209 and 0.03 bar, respectively.

diffusion barriers for the migrating oxygen ions/vacancies which is in agreement with the finding of Ref. [21]. However, different grain sizes can also influence the process of surface exchange as discussed in Refs. [22,23] so that a grain size dependent surface kinetics cannot be excluded.

3.3. Micro- and ultrastructure of grain boundaries in perovskite ceramics by TEM

To elucidate the real structure of membrane materials from the micrometer down to the sub-nanometer scale TEM is an indispensable tool. The usefulness of which is illustrated in the case of two model perovskite materials of practical importance.

Fig. 4 shows TEM investigations on the microstructure of a BCFZ ceramic sintered in disk geometry above 1200 °C. The bright- and dark-field micrographs in Fig. 4a and b reveal the size of the BCFZ grains to be of the order of 500 nm. BF and DF were taken with an objective aperture that collects electrons in an half angle of 7.5 mrad; the position relative to the diffraction pattern is indicated for the dark field conditions by a circle in Fig. 4c. The DF shows no indication of intergranular glass what would be clearly visible by continuous bright lines along the grain boundaries [24]. Instead, the grain boundaries are decorated by smaller crystallites with sizes less than 100 nm that were found by SAED and EDXS to be most probably a BCFZ perovskite with a high Zr content. The diffraction pattern in Fig. 4c was taken of a circular region of 1.2 μm in diameter that contained perovskite grains as well as grain boundaries. The relatively small and randomly oriented grain boundary crystals give rise to the appearance of Debye–Scherrer rings. The diameters of the best developed ones correspond to lattice plane distances of 0.3 and 0.18 nm that match well to the (1 1 1) and (2 1 0) planes of BCFZ perovskite with a high Zr content, respectively. EDX spectra of the large perovskite grains showed Ba, Co, Fe, Zr, and O (Fig. 4d). In the spectra from the grain boundary regions with a high concentration of the small high-Zr BCFZ perovskite the Zr–L lines at around 2 keV (marked by stars) show up with much higher intensity, but strong signals of Co and Fe are still present (Fig. 4e). The two-phase characteristic of the BCFZ perovskite was already present in the starting powder. In X-ray powder diffractograms [13], perovskite reflexes show up always as doublets and indicate a lattice deviation of a few percent between these two $Ba(Co,Fe,Zr)O_{3-\delta}$ perovskite phases.

Fig. 5 shows an example of an accommodation of grains in a BSZF ceramic with the absence of any grain boundary phase. The polycrystalline perovskite type material consists of grains of different crystallographic orientation and, consequently, at the grain boundaries a lattice misfit occurs. As an example, Fig. 5a shows the grain boundary with a large misfit f [25] of 45% between the (0 1 1) planes of grain A and the (0,1,−2) planes of grain B:

$$f = \frac{d_{011} - d_{0,1,-2}}{1/2(d_{011} + d_{0,1,-2})} = \frac{0.291\,\text{nm} - 0.184\,\text{nm}}{1/2(0.291\,\text{nm} + 0.184\,\text{nm})} = 45\%$$

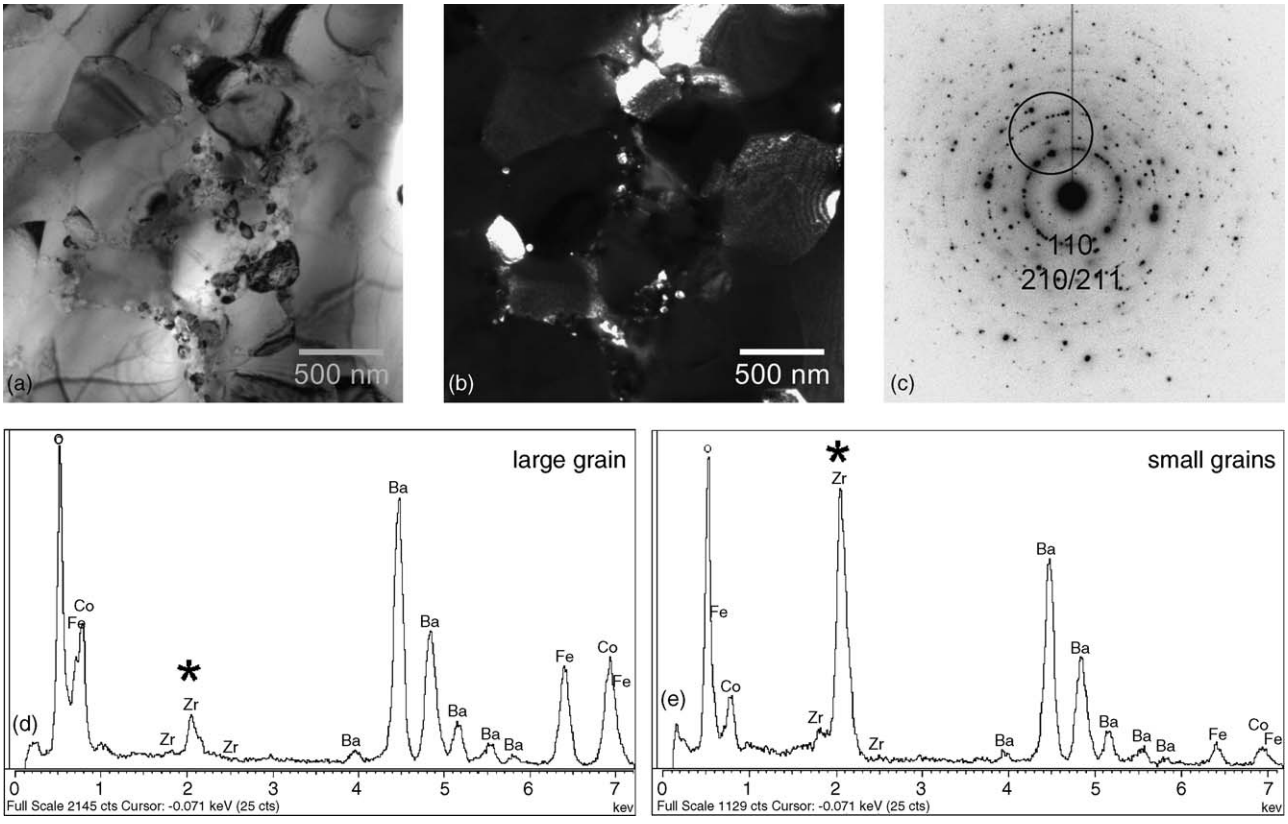

Fig. 4. Microstructure of a BCFZ ceramic: (a) TEM bright-field, (b) TEM dark-field, (c) selected area electron diffraction, (d) EDXS of perovskite grain, and (e) EDXS of grain boundary region.

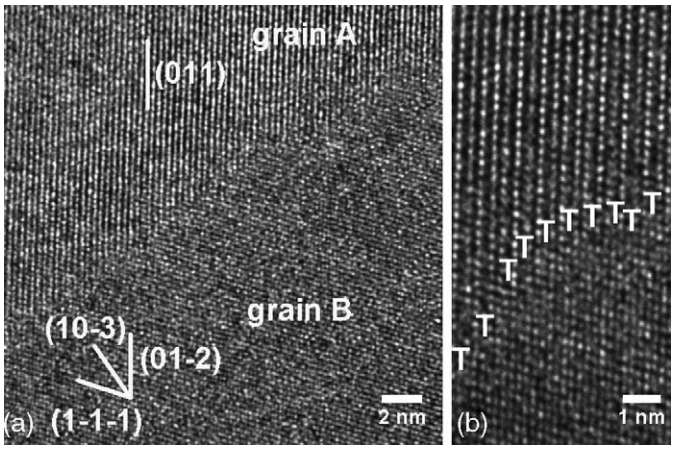

Fig. 5. HRTEM study of a grain boundary in a BSZF ceramic. (a) Two adjacent grains with misfit between (0 1 1) and (0,1,−2) planes; (b) indication of misfit dislocations by T's.

The misfit is accommodated by misfit dislocations (marked by T's in Fig. 5) rather than by lattice strain. This misfit strain can cause thermal expansion induced microcracking. It was found that at very small misfit strains, the large grain microstructure develops microcracks before the small grain microstructure [26]. In other examples using HRTEM the strain fields of edge-type misfit dislocations in ferroelectric perovskites could be visualized [27] and the atomic structure of misfit dislocations in $SrZrO_3$ type perovskites were studied [28]. It seems to be characteristic of perovskite ceramics that the strain caused by the misfit is reduced by the incorporation of lattice plane dislocations. As shown in Fig. 5b, for every third (0,1,−2) lattice plane of grain B a misfit dislocation is observed that marks an unpaired atomic plane.

3.4. Thermal expansion

For the proper handling of membranes in gas separation modules and membrane reactors we need information on their thermal expansion behaviour. Fig. 6 shows the lattice constants of BCFZ, BSCF and SCF perovskite powder at various temperatures determined from *in situ*—XRD measurements in air. From Fig. 6 it can be seen that the lattice constants of the three perovskites under study almost linearly increase with temperature. The thermal expansion coefficients (TEC) can be calculated, therefore, using the definition $d(\Delta a/a_0)/dT$ (*a:* lattice constant, a_0: lattice constant at room temperature). From Fig. 6, the average TEC of BCFZ, BSCF and SCF were obtained to be (10.3, 11.5 and 15.6) $\times 10^{-6}\,K^{-1}$, respectively. The perovskites BSCF and SCF show higher TEC than BCFZ with a much lower Co content. Co-rich mixed conducting membranes usually have high TEC, which is mainly due to the large ion radius variation of cobalt between 2+ and 4+ oxidation state (the ionic radius of Co^{2+}, Co^{3+}, Co^{4+} are 88.5, 75 and 68.5 pm). The highest thermal expansion coefficient is found for SCF. This high thermal expansion of SCF is due to the high concentration of cobalt and iron which can easily change their valences in this composition. It can be assumed that the higher the thermal expansion coefficient of the perovskite is, the more easily the B-side ions can change their valences. The relationship between reducibility and the thermal expansion coefficient is also validated by comparing the BSCF and BCFZ materials. It is found that doping the B-site of perovskites with metal cations exhibiting a constant oxidation state, such as Zr^{4+}, can suppress oxygen nonstoichiometry variations and lattice expansion [29]. From our experiments it was found that the thermal expansion coefficient of BCFZ ($10.3 \times 10^{-6}\,K^{-1}$) is lower than that of BSCF ($11.5 \times 10^{-6}\,K^{-1}$). This finding is in agreement with the fact that the membrane reactor made of BCFZ is more stable during the partial oxidation of methane to synthesis gas than that made of BSCF [30].

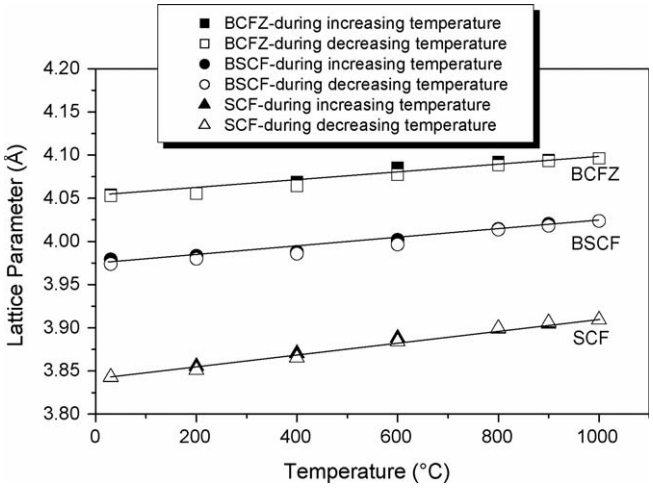

Fig. 6. Temperature dependence of the lattice constants of BCFZ, BSCF and SCF powder in air.

3.5. Applications

3.5.1. Production of O_2

There are two main goals for the production of pure oxygen at a high temperature level: oxygen for power plants with CO_2 sequestration and oxygen for catalytic partial oxidations.

Among the different concepts for CO_2 capture in the effluent gas of power stations, the concept based on the individual steps: (i) coal gasification, (ii) burning this gas in a gas turbine, (iii) steam turbine, and (iv) treatment of the effluent gases by water condensation seems to be most promising. The remaining effluent gas is almost pure CO_2. This concept requires N_2-free oxygen in the coal gasification step. Fig. 7 shows that the BCFZ hollow fibres with a wall thickness of ca. 175 μm produces under comparable experimental conditions, that is to say using inert sweep gases, higher oxygen fluxes than the other oxygen transporting membranes known so far. In our case He was used as sweep gas which is, however, not applicable under industrial conditions. In the power plant concept with CO_2 sequestration, a part of the effluent gas is used as sweep gas, i.e. the sweep gas for the oxygen separator consists of about 80 vol.% CO_2 and 20 vol.% steam. This concept requires steam and CO_2 resistant Ba-, Sr-free membranes. Whereas the BCFZ perovskite used for the hollow fibre preparation in this paper is not stable at high CO_2

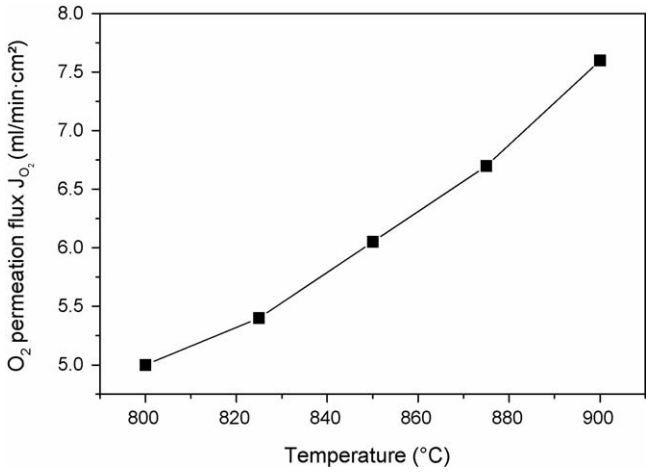

Fig. 7. Oxygen permeation flux through a BCFZ hollow fibre membrane as a function of temperature. Experimental conditions: air flow on the core side = 150 ml/min; He as sweep on the shell side = 30 ml/min; length of the fibre = 11.9 mm; outer diameter of the fibre = 0.88 mm; inner diameter = 0.53 mm. Sealing of the short fibre with Au paste. The oxygen partial pressures on the air side and on the sweep side are 0.209 and 0.06 bar, respectively.

concentrations due to $BaCO_3$ formation, for CO_2-rich sweep gases perovskites like doped La–Ni oxides can be used [31].

3.5.2. Production of O_2 enriched air

Here we propose a novel technique to produce O_2-enriched air by transporting oxygen from slightly pressurized air through a BCFZ perovskite hollow fibre membrane to air of lower pressure thus increasing the oxygen content of this air to typically 40–50 vol.% O_2 [32]. So the perovskite membrane integrates the *in situ* oxygen supply with the mixing of the permeated oxygen with air in one unit thus reducing the apparatus costs.

Fig. 8 shows the influence of the temperature on the O_2-enrichment under a fixed pressure difference of 1.5 bar. As expected, the oxygen permeation rate increases with rising temperature, which leads both to an increase of the production rate of O_2-enriched air and of the O_2 concentration in the effluent air. Because of the high O_2-selectivity of the BCFZ hollow fibre membrane we have no enrichment of inert gases like Ar or CO_2. Another advantage of BCFZ hollow fibre membranes is their relative high O_2-flux and the resulting high production rate of O_2-enriched air in comparison with hollow fibre organic polymer membranes. A typical silicon rubber membrane of 25 μm thickness shows an oxygen permeability of 0.11 ml/min cm^2 and a separation factor O_2:N_2 = 2.25, and about 10 bar pressure difference are necessary to produce 35 vol.% O_2-enriched air [33].

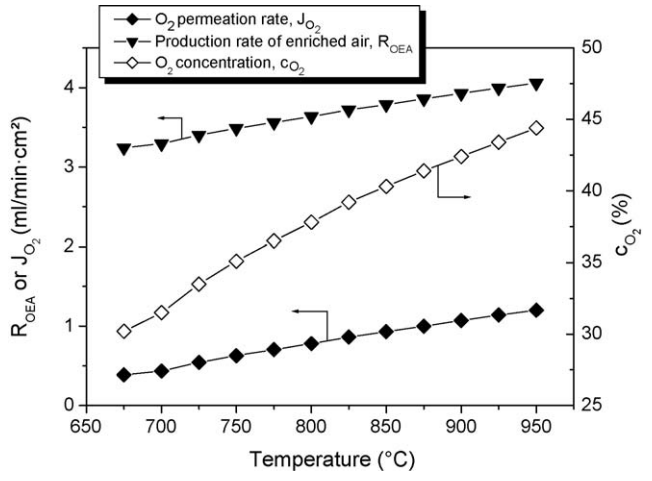

Fig. 8. Influence of temperatures on the production of O_2-enriched air using BCFZ hollow fibre membranes. Experimental conditions: air flow rate as feed on the core side = 100 ml/min; air flow rate as sweep on the shell side = 10 ml/min; pressure difference = 1.5 bar; membrane surface area = 3.5 cm^2; pressure difference = 1.5 bar. Thirty centimetres long fibre, 16 cm were regarded as effective fibre length at a temperature >500 °C (from the temperature profile of the 24 cm long oven).

In this mode of oxygen enrichment, stability problems do not occur since both sides of the BCFZ perovskite membrane were exposed to an oxidizing atmosphere (air). As expected, the perovskite membranes exhibit an excellent stability as shown in Fig. 9. The perovskite membrane was operated steadily for more than 800 h at 875 °C under 1.5 bar air pressure difference. During the long-time operation, the oxygen concentration in the O_2-enriched air reaches around 42 vol.% with an oxygen permeation rate of ∼1.0 ml/min cm^2 and an O_2-enriched air production rate of ∼4.0 ml/min cm^2. It should be pointed out that we have stopped the long-term testing although the perovskite membrane was still working after 800 h. This operational mode to get O_2-enriched air is quite different from producing pure oxygen by perovskite membranes with a re-circulating condensable inert gas (such as steam). In the latter case the low O_2 partial pressure (≤1 vol.%) on the sweep side of the membrane can lead to a slow degradation of the perovskite structure.

3.5.3. Partial oxidations in oxygen transporting membrane reactors

Reactors with oxygen transporting membranes in combination with an oxidation catalyst are promising tools for partial

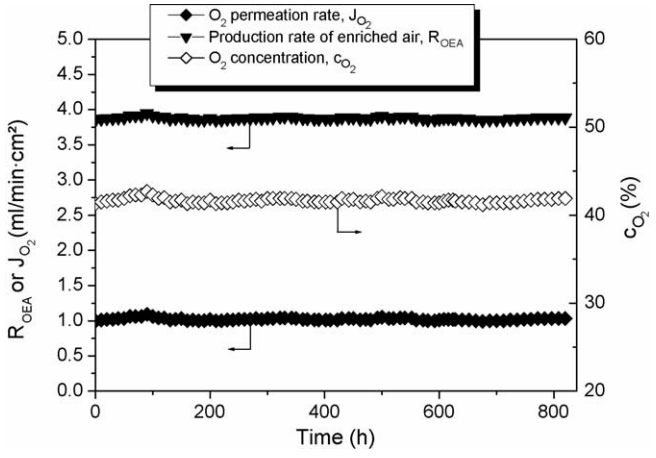

Fig. 9. Long-time stability of BCFZ perovskite hollow fibres in the production of O_2-enriched air. Experimental conditions: air flow rate as feed on the core side = 100 ml/min; air flow rate as sweep on the shell side = 10 ml/min, membrane surface area = 3.5 cm^2; pressure difference = 1.5 bar; T = 875 °C. Thirty centimetres long fibre, 16 cm were regarded as effective fibre length at a temperature >500 °C (from the temperature profile of the 24 cm long oven).

oxidations such as oxi-dehydrogenations of alkanes to the corresponding alkenes or oxidative coupling reactions of methane to C_2 hydrocarbons. However, these applications require defined short contact times to avoid a deeper oxidation of the desired hydrocarbons (see Wang et al., this issue).

The problem of deeper oxidation plays also a role in the methane transformation to synthesis gas (CO and H_2) as shown in Fig. 10 using BCFZ hollow fibre membranes. Two major mechanisms of POM are discussed in literatures [34,35], the reforming mechanism at low WHSV (WHSV: weight hourly space velocity) [34] and the direct partial oxidation mechanism at high WHSV [35]. There is experimental evidence that under

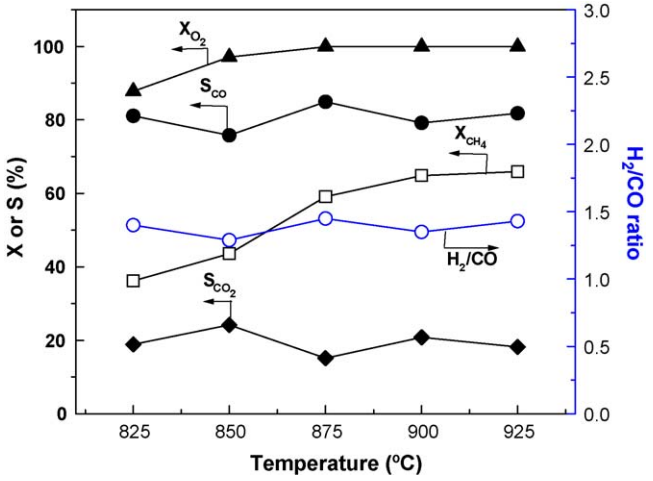

Fig. 10. Conversion of methane and oxygen and the selectivity of CO formation in the POM reaction as a function of temperature using one BCFZ hollow fibre membrane in the membrane reactor. Experimental conditions: air flow on the core side = 150 ml/min; CH_4 flow on the shell side = 60 ml/min; surface area of the BCFZ hollow fibre = 3.5 cm^2; amount of the $LaMnNiO_x/\alpha$-Al_2O_3 catalyst = 1.4 g. Thirty centimetres long fibre, 16 cm were regarded as effective fibre length at a temperature >500 °C (from the temperature profile of the 24 cm long oven).

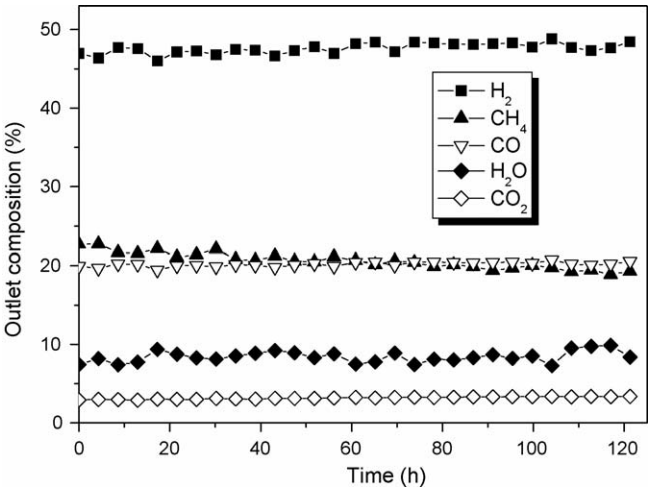

Fig. 11. Production of synthesis gas by partial oxidation of methane in a BCFZ laboratory hollow fibre membrane reactor at 850 °C. Core side: air; shell side: CH_4. Thirty centimetres long fibre, 16 cm were regarded as effective fibre length at a temperature >500 °C (from the temperature profile of the 24 cm long oven).

our conditions methane is first deeply oxidized to CO_2 and H_2O and then these products of total oxidation react with methane giving synthesis gas (CO, H_2). Therefore, in the so-called ''partial'' oxidation of methane to synthesis gas the classical steam reforming (SR) catalysts are used. H_2O and CO_2 become reduced by unreacted CH_4 in SR and dry reforming to CO and H_2 using established Ni-based SR catalysts. Consequently, Chen et al. [36] called the synthesis gas formation in a perovskite membrane reactor an ''oxidation-reforming process''. The oxidation processes not only include the deep oxidation of methane to CO_2 and steam but also, of course, include the oxidation of H_2 and CO to CO_2 and H_2O. The reforming processes include the dry reforming and steam reforming. In our experiments (Fig. 10) the H_2/CO ratio at 825 °C is 1.8 and it continues to decrease with increasing temperature to about 1.6 at 925 °C since the oxygen entering the reactor is not only used for increasing the methane conversion but also for the burning of the hydrogen produced. The same experimental finding was made by Ref. [36] with an H_2/CO ratio of 1.8.

Fig. 11 shows an example for the production of synthesis gas by partial oxidation of methane in a BCFZ laboratory hollow fibre membrane reactor at 850 °C. The gas composition at the reactor outlet was 55 vol.% H_2, 23 vol.% CO, 4 vol.% CO_2, 11 vol.% H_2O, 7 vol.% CH_4, which corresponds to 82.5% CO selectivity at 79.4 CH_4 conversion with a H_2/CO ratio of 2.39. By increasing the amount of catalyst or applying a SR catalyst of higher activity or having a packed bed SR catalyst behind the membrane reactor as proposed by Ref. [36], the H_2 and CO content in this outflow gas can be increased on the expense of CH_4, CO_2 and H_2O. By using a Ni-based SR catalyst deposited after the BCFZ hollow fibre membrane in the direction of the reactor outlet, all CO_2 and H_2O could be transformed with a fine-tuned amount of unreacted CH_4 by reforming steps to synthesis gas with a CO-selectivity of >97% and a H_2/CO ratio ≈2 [37].

4. Conclusions

Because of their relative thin walls the BCFZ hollow fibres show an extremely high O_2 flux. At 850 °C for a wall thickness of 175 μm an O_2 flux of 6 ml/min cm^2 was measured using He as inert sweep gas and having an Au-sealed short piece of the hollow fibre in the isothermal zone of the oven. When the oxygen partial pressure is further decreased by the presence of CH_4 in catalytic reactor experiments, the driving force for O_2 transport is increased and the O_2 fluxes become even higher. Long time tests in various gas atmospheres proved that the material BCFZ shows not only a relative high O_2 flux but also a good stability.

The studies of the microstructure indicate that a large grain size increases the oxygen permeability. Doping the B-site with cations of constant oxidation state reduces the thermal expansion coefficient. In contrast, cations with variable oxidation states of different ionic radii enlarge it.

The advantages of the hollow fibre geometry with a high ratio of membrane area to the permeator volume allow the application of these fibres in separators and catalytic membrane reactors. When arranged in bundles, a high membrane area per

reactor/permeator volume can be achieved. Economic goals, e.g. membrane area/m^3 permeator of the order of 5000 m^2 at a price of well below €1000 m^{-2} are met by the perovskite hollow fibres. Based on our results, the oxygen necessary for a methanol-plant with a capacity of 2000 tonnes/day based on partial oxidation of methane could be delivered by a bunch of 4,600,000 fibres. Assuming a fibre length of 1 m, this would lead to a relatively small cylindrical module with a diameter of roughly 2 m (depending on the packing of the fibres). When comparing this volume to a classical air separation unit, the enhancement in space–time–yield (in terms of oxygen per plant size) is obvious.

Acknowledgements

The authors thank the German Federal Ministry of Education and Research for the financial support of the project CaMeRa (Catalytic Membrane Reactor) under the auspices of ConNeCat (Competence Network Catalysis). H. Wang thanks the Humboldt Foundation for financial support.

References

[1] Y. Teraoka, H.M. Zhang, S. Furukawa, N. Yamazoe, Chem. Lett. 11 (1985) 1743.
[2] Y. Teraoka, T. Nobunaga, N. Yamazoe, Chem. Lett. 3 (1988) 503.
[3] X. Tan, Y. Liu, K. Li, AIChE J. 51 (2005) 1991.
[4] X. Tan, Y. Liu, K. Li, Ind. Eng. Chem. Res. 44 (2005) 61.
[5] X. Tan, Y. Liu, K. Li, J. Membr. Sci. 188 (2001) 87.
[6] S. Liu, X. Tan, K. Li, R. Hughes, J. Membr. Sci. 193 (2001) 249.
[7] S. Liu, K. Li, R. Hughes, Mater. Res. Bull. 39 (2004) 119.
[8] S. Liu, G.R. Gavalas, J. Membr. Sci. 246 (2005) 103.
[9] S. Liu, G.R. Gavalas, Ind. Eng. Chem. Res. 44 (2005) 7633.
[10] T. Schiestel, M. Kilgus, S. Peter, K.J. Caspary, H. Wang, J. Caro, J. Membr. Sci. 258 (2005) 1.
[11] M. Trunec, J. Eur. Ceram. Soc. 24 (2003) 645.
[12] J. Luyten, A. Buekenhoudt, W. Adriansens, J. Cooymans, H. Weyten, F. Servaes, R. Leysen, Solid State Ionics 135 (2000) 637.
[13] C. Tablet, G. Grubert, H.H. Wang, T. Schiestel, M. Schroeder, B. Langanke, J. Caro, Catal. Today 104 (2005) 126.
[14] J.H. Tong, W.S. Yang, R. Cai, B.C. Zhu, L.W. Lin, Catal. Lett. 78 (2002) 129.
[15] W. Yang, et al., Chinese Patent 00136198.8 (2000).
[16] Z.P. Shao, W.S. Yang, Y. Cong, H. Dong, J.H. Tong, G.X. Xiong, J. Membr. Sci. 172 (2000) 177.
[17] H.H. Wang, C. Tablet, G. Grubert, A. Feldhoff, J. Caro, Adv. Mater. 17 (2005) 1785.
[18] H.H. Wang, J. Caro, C. Tablet, G. Grubert, EPA 04020506 (April 6, 2005).
[19] H. Kruidhof, H.J.M. Bouwmeester, R.H.E. VanDoorn, A.J. Burggraaf, Solid State Ionics 63–65 (1993) 916.
[20] K. Zhang, Y.L. Yang, A.J. Jacobson, K.S. Salama, J. Mater. Sci. 34 (1999) 1367.
[21] V.V. Kharton, F.M.B. Marques, Curr. Opin. Solid State Mater. Sci. 6 (2002) 261.
[22] H.J.M. Bouwmeester, H. Kruidhof, A.J. Burggraaf, Solid State Ionics 72 (1994) 185.
[23] K. Huang, J.B. Goodenough, J. Electrochem. Soc. 148 (2001) E203.
[24] A. Feldhoff, M.F. Trichet, L. Mazerolles, M. Backhaus-Ricoult, J. Eur. Ceram. Soc. 25 (2005) 1733.
[25] J.H. van der Merwe, Crit. Rev. Solid State Mater. Sci. (1978) 209.
[26] N. Sridhar, W. Yang, D.J. Srolovitz, E.R. Fuller, J. Am. Ceram. Soc. 77 (1994) 1123.
[27] M.W. Chu, I. Szafraniak, R. Scholz, C. Harnagea, D. Hesse, M. Alexe, U. Gösele, Nat. Mater. 3 (2004) 87.
[28] F. Ernst, M. Ruehle, A. Recnik, P.A. Langjahr, P.D. Nellist, Acta Mater. 47 (1998) 183.
[29] V.V. Kharton, V.A. Sobyanin, V.D. Belyaev, G.L. Semin, S.A. Veniaminov, E.V. Tsipis, A.A. Yaremchenko, A.A. Valente, I.P. Marozau, J.R. Frade, J. Rocha, Catal. Commun. 5 (2004) 311.
[30] H.H. Wang, Y. Cong, W.S. Yang, Catal. Today 82 (2003) 157.
[31] C. Li, G. Yu, N. Yang, Sep. Purif. Technol. 32 (2003) 335.
[32] H.H. Wang, S. Werth, T. Schiestel, J. Caro, Angew. Chem. Int. Ed. 44 (2005) 6906.
[33] S.L. Matson, W.J. Ward, S.G. Kimura, W.R. Browall, J. Membr. Sci. 29 (1986) 79.
[34] D. Dissanayake, M.P. Rosynek, K.C.C. Kharas, J.H. Lunsford, J. Catal. 132 (1991) 117.
[35] D.A. Hickman, L.D. Schmidt, Science 259 (1993) 343.
[36] C. Chen, S. Feng, S. Ran, D. Zhu, W. Liu, H.J.M. Bouwmeester, Angew. Chem. Int. Ed. 42 (2003) 5196.
[37] H.H. Wang, C. Tablet, T. Schiestel, S. Werth, J. Caro, Catal. Commun., in press.